

Technical Note

An Atmospheric Correction Method over Bright and Stable Surfaces for Moderate to High Spatial-Resolution Optical Remotely Sensed Imagery

Bo Zhong ^{1,2} , Shanlong Wu ¹, Aixia Yang ^{1,*}, Kai Ao ², Jinhua Wu ³, Junjun Wu ¹, Xueshuang Gong ⁴, Haibo Wang ⁴ and Qinhuo Liu ¹ 

¹ State Key Laboratory of Remote Sensing Science, Aerospace Information Research Institute, Chinese Academy of Sciences, Beijing 100101, China; zhongbo@radi.ac.cn (B.Z.); wusl420056@aircas.ac.cn (S.W.); wujj@radi.ac.cn (J.W.); liuqh@radi.ac.cn (Q.L.)

² College of Computer Science and Technology, Chongqing University of Posts and Telecommunications, Chongqing 400065, China; s180201046@stu.cqupt.edu.cn

³ School of Earth Sciences and Resources, China University of Geosciences, Beijing 100083, China; 2001170269@cugb.edu.cn

⁴ China Centre for Resources Satellite Data and Application, Beijing 100094, China; gongxueshuang@chinasat.com (X.G.); wanghaibo@chinasat.com (H.W.)

* Correspondence: yangax@radi.ac.cn; Tel./Fax: +86-10-64806256

Received: 3 February 2020; Accepted: 17 February 2020; Published: 22 February 2020



Abstract: Although many attempts have been made, it has remained a challenge to retrieve the aerosol optical depth (AOD) at 550 nm from moderate to high spatial-resolution (MHSR) optical remotely sensed imagery in arid areas with bright surfaces, such as deserts and bare ground. Atmospheric correction for remote-sensing images in these areas has not been good. In this paper, we proposed a new algorithm that can effectively estimate the spatial distribution of atmospheric aerosols and retrieve surface reflectance from moderate to high spatial-resolution imagery in arid areas with bright surfaces. Land surface in arid areas is usually bright and stable and the variation of atmosphere in these areas is also very small; consequently, the land-surface characteristics, specifically the bidirectional reflectance distribution factor (BRDF), can be retrieved easily and accurately using time series of satellite images with relatively lower spatial resolution like the Moderate-resolution Imaging Spectroradiometer (MODIS) with 500 m resolution and the retrieved BRDF is then used to retrieve the AOD from MHSR images. This algorithm has three advantages: (i) it is well suited to arid areas with bright surfaces; (ii) it is very efficient because of employed lower resolution BRDF; and (iii) it is completely automatic. The derived AODs from the Multispectral Instrument (MSI) on board Sentinel-2, Landsat 5 Thematic Mapper (TM), Landsat 8 Operational Land Imager (OLI), Gao Fen 1 Wide Field Viewer (GF-1/WFV), Gao Fen 6 Wide Field Viewer (GF-6/WFV), and Huan Jing 1 CCD (HJ-1/CCD) data are validated using ground measurements from 4 stations of the AEROSOL ROBOTIC NETWORK (AERONET) around the world.

Keywords: AOD; moderate to high spatial resolution; atmospheric correction; AERONET; automatic; validation

1. Introduction

A large number of continental- and global-scale applications at 30 m resolution have been created and have pushed the discoveries using remote sensing at higher spatial resolution forward, since the Landsat series of satellite data have been made freely downloadable. These applications include the Finer Resolution Observation and Monitoring of Global Land Cover project [1], the Global Forest

Cover Change [2], etc. With increasing moderate to high spatial-resolution (MHSR) optical data available, the research and applications with higher spatial resolution at global scale is dramatically increasing. In particular, the satellite constellations with higher spatial resolution optical sensors will dramatically increase the observations with higher resolution, such as the Sentinel2 Multispectral Instrument (MSI) of European Space Agency (ESA), the Chinese GaoFen 1 (GF1) and GaoFen 6 (GF6) Wide Field Viewers (WFOVs), and so on. However, the atmospheric effect on optical remote-sensing imagery usually degrades the applications and the temporal and spatial variation of aerosols are very difficult to completely remove [3,4].

A better surface reflectance dataset with spatial and temporal consistency at global scale has been required by the global-scale applications at higher spatial resolution and some methods have been developed for this purpose, such as the Landsat Ecosystem Disturbance Adaptive Processing System (LEDAPS) algorithm [5] and the Moderate-resolution Imaging Spectroradiometer (MODIS)-based algorithms [6,7]. Firstly, both of the methods used the MODIS aerosol optical depth (AOD) product [8–10] with a lower spatial resolution of 7–10 km, which is only 1/20–1/30 of the required resolution, and a large portion of void areas, especially arid areas, were interpolated; subsequently, the spatial distribution of aerosols at high resolution (30 m and higher) cannot be captured well, which causes spatial inconsistency. In addition, the situations in arid areas were not taken into consideration, which largely degraded the applications in these areas.

For MHSR remote-sensing data, the dark target (DT) method [11] including dense dark vegetation (DDV) [8] is the most used and only partial areas of an image with dark objects are used to retrieve the AOD, which fails at areas without dense vegetation or shadow. The contrast reduction (CR) method [12] is developed specifically for stable surface and it use the variation of aerosol over stable surface from multi-temporal images to extract AOD; however, it needs a clear image as a reference, or it fails. ImAero-Landsat [13] is a hybrid method by integrating DDV and contrast reduction; the shortcoming of the contrast reduction method is not avoidable. The histogram-matching method [14] needs the identification of clear regions in an image in the first place, which is very difficult for automation and usually requires manual intervention [14]. Thus, the AOD retrieval and atmospheric correction for images over arid areas with bright surfaces remains a challenge. The method based on spatial expansion [15] has partially solved this problem; however, some images with very high resolution containing only bright surfaces will fail because of no initial AOD retrieved.

In order to automatically retrieve accurate AOD over arid areas with bright surfaces from MHSR remotely sensed imagery, we present a new method that can better estimate the aerosols and retrieve surface reflectance from MHSR imagery in arid areas with bright surfaces. Land surface in arid areas is usually bright and stable and the variation of atmosphere in these areas is also very small; consequently, the land-surface characteristics, specifically the bidirectional reflectance distribution factor (BRDF), can be retrieved easily and accurately using time series of satellite images with relatively lower spatial resolution like MODIS with 500 m resolution and the retrieved BRDF is then used to retrieve the AOD from MHSR images. The derived AODs from Sentinel-2/MSI, Landsat 8 Operational Land Imager (OLI), and GF-1/WFOVs are validated using ground measurements from 4 sites of the AEROSOL ROBOTIC NETWORK (AERONET) around the world. The validation indicates that this method is very good in arid areas for MHSR imagery.

2. Materials and Methods

2.1. Moderate to High Spatial-Resolution (MHSR) Remotely Sensed Data

In this study, the proposed method can be applied to most of the MHSR data. These data include the Thematic Mapper (TM), the Enhanced Thematic Mapper (ETM+), and the Operational Land Imager (OLI) onboard the Landsat series of satellites, the Multispectral Imager (MSI) on Sentinel-2, the Charge-Coupled Device (CCDs) on HuanJing 1 (HJ-1), the Wide Field Viewer (WFOV) on Gao Fen (GF) 1 and 6, the MSI on ZiYuan 3 (ZY3), the CCD and World Field Imager (WFI) on the Chinese and

Brazil Earth Resource Satellite 02B (CBERS-02B), and so on. More MHSR data can be included after adaptative modification. Only data from the Landsat series and Sentinel-2 satellites have shortwave infrared (SWIR) band and all the data have visible and near infrared (VNIR) bands. Table 1 shows the details of the above MHSR data.

Table 1. The details of the moderate to high spatial-resolution (MHSR) data are used in this study ¹.

Sensor(s)	Platform(s)	Spatial Resolution (m)	Swath (km)	Spectra for AOD Retrieval	Nation
TM, ETM+, OLI	Landsat	30	185	VNIR, SWIR	USA
MSI	Sentinel-2	10/20/60	290	VNIR, SWIR	ESA
CCD	HJ-1/A&B	30	700 (2 cameras)	VNIR	China
CCD	CBERS-02B	20	113	VNIR	China
WFI		2.36	27		
CCD	GF-1	8	60	VNIR	China
WFV		16	800 (4 cameras)		
MSI	ZY-3	5.8	52	VNIR	China
CCD	GF-6	8	60	VNIR	China
WFV		16	800 (1 camera)		
MODIS	Terra/Aqua	250/500/1000	2330	VNIR, SWIR	USA

¹ Abbreviations: TM, Thematic Mapper; ETM+, Enhanced Thematic Mapper; OLI, Operational Land Imager; CCD, Charge-Coupled Device; WFI, World Field Imager; WFV, Wide Field Viewer; GF-1, GaoFen 1; ZY-1, ZiYuan 1; GF-6, GaoFen 6; AOD, aerosol optical depth; VNIR, Visible and near infrared bands; SWIR, short-wave infrared bands.

2.2. Methodology

The basic theory of the proposed algorithm is very similar to that of the CR method [16] and they are all developed for the arid areas with bright and stable surfaces. The assumption is that the land surface is very stable so that the variation of top of atmosphere (TOA) reflectance is completely induced by the variation of atmosphere alone. Subsequently, the CR method chooses one image least contaminated by the atmosphere from multi-temporal images as reference and the AODs for other images are retrieved by quantifying the variations induced by aerosols. Two problems immediately emerge while applying CR method to the MHSR data and the problems are described as follows:

- (1). It is not easy to select the clearest images from multi-temporal images automatically;
- (2). For most of the Chinese MHSR data having very wide swath, the reflectance difference induced by BRDF is aggregated into the retrieved AOD while choosing one clear image as reference and the difference can reach as high as 15% in extreme cases [17]; the retrieved AOD is consequently degraded.

In order to solve the above two problems for better retrieval of AOD from MHSR data, we propose a new algorithm which uses multi-year time series of MODIS data from both Terra and Aqua to construct the BRDF of arid areas with bright and stable surface in advance. The pre-constructed BRDF then supports the AOD retrieval from the MHSR data with much higher accuracy. The procedure of the proposed method is illustrated in Figure 1.

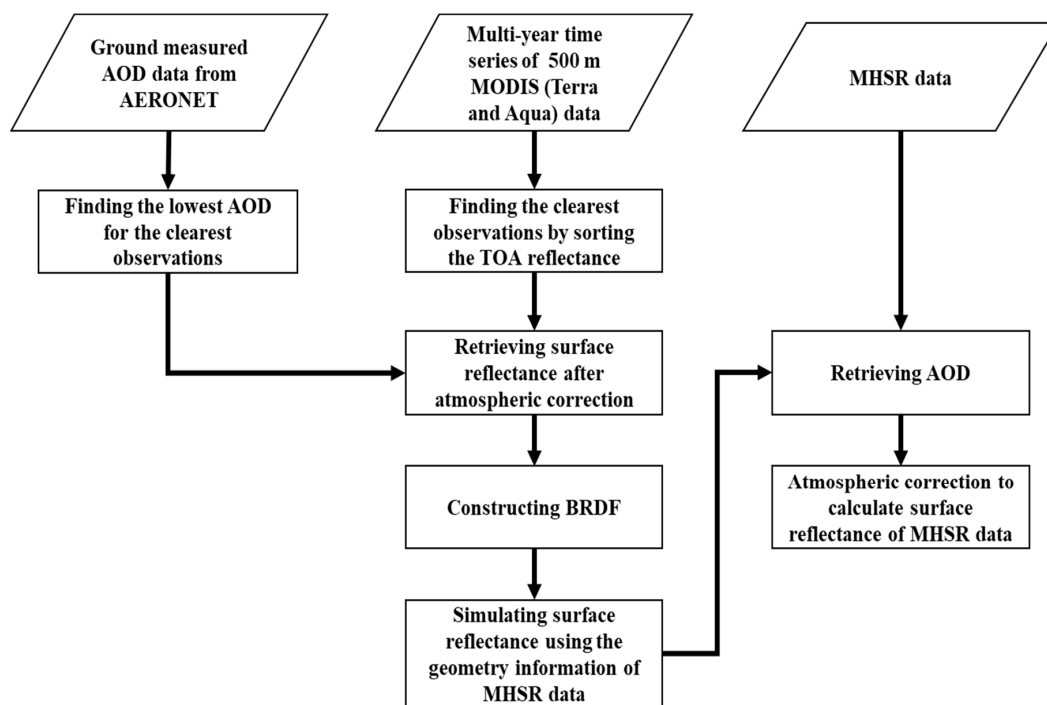


Figure 1. Flowchart of the new aerosol optical depth (AOD) retrieval method.

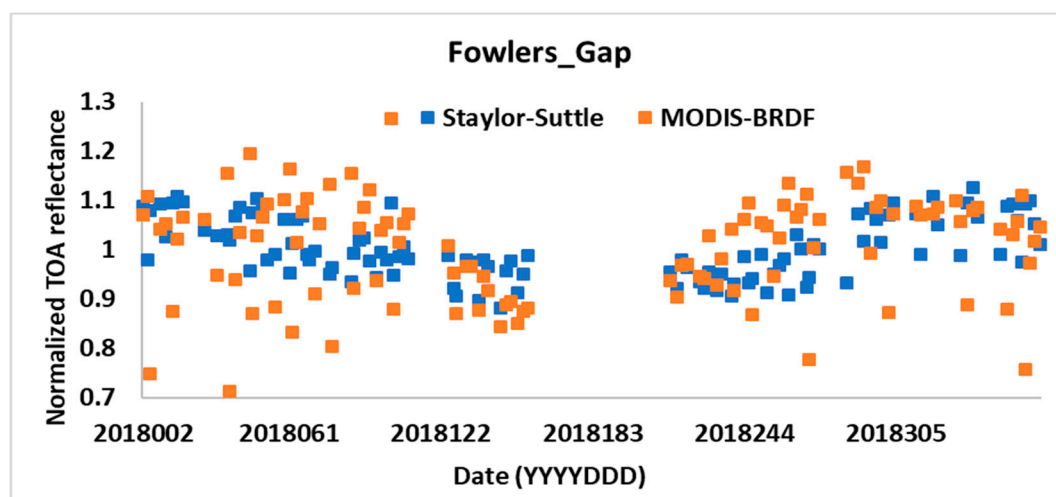
2.2.1. The Retrieval of the Bidirectional Reflectance Distribution Factor (BRDF) Characterization

The key process of the proposed method is the retrieval of the BRDF characterization. For a stable surface, the BRDF characterization is very constant, so it can be retrieved through time-series analysis using large amount of historical data, such as the method proposed in [16,18]. Although the method in [16,18] has been proved effective in some scenarios [16], some problems still remain; therefore, some key improvements are subsequently proposed in this study to retrieve better BRDF and the following atmospheric correction in arid areas. Three improvements are made as follows:

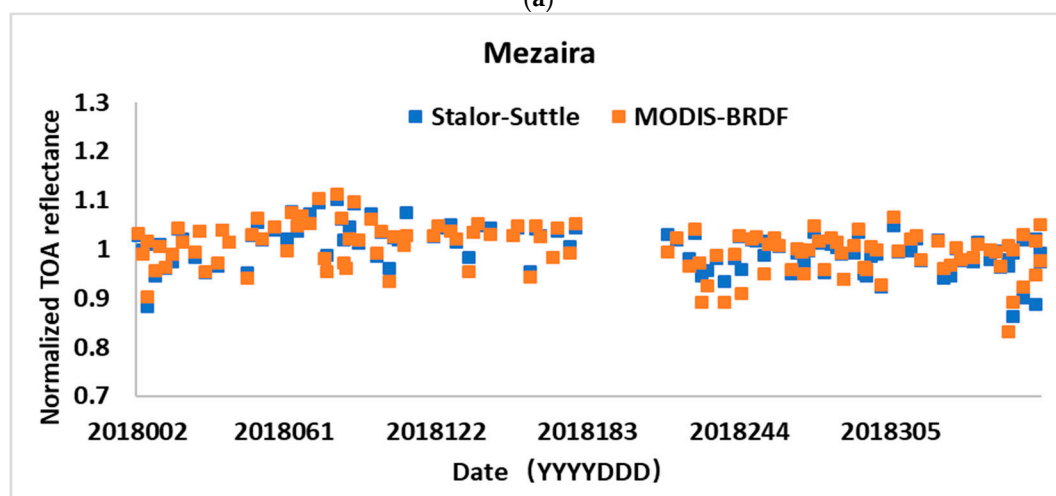
- (1). Instead of being applied to all land surfaces, the proposed method is only for the arid areas with bright and stable surfaces; the stability of the land surface enables use of much longer temporal range to retrieve more data to fit the BRDF characterization and subsequently improve the fitting accuracy of the BRDF characterization. Therefore, instead of using 1 km MODIS data within only one year, the proposed method uses a multi-year time-series dataset composed of 500 m MODIS data from both Terra and Aqua, which has higher resolution and a longer temporal period; thus, higher resolution means more detail and a multi-year time series dataset retrieves more “clearest” observations which captures better the BRDF characterization. Whether the AOD’s resolution of 500 m from MODIS data is enough for atmospheric correction of MHSR data needs to be clarified before moving on; the method is only applied to the arid areas, such as desert and the Gobi, where the spatial variation of aerosol is usually very small, so 500 m is a suitable resolution of AOD retrieval, which can also greatly improve the algorithm’s efficiency.
- (2). Due to the path becoming longer with the increasing of view zenith angle, the TOA reflectance increases; however, the view zenith angle (VZA) is not taken into consideration while choosing the clearest observations and most of the clearest observations concentrate on observations with smaller VZA, which may cause large error. Thus, the proposed method chooses the clearest observations for every 10 degrees’ interval of VZA from 0 to 40 degrees (0–10, 11–20, 21–30, and 31–40), which will obtain observations with an even distribution of VZAs and subsequently improve the accuracy of the simulated BRDF. In addition, VZAs of MHSR data are seldom larger than 40 degree. Zhong et al. [17] undertook an accuracy evaluation of different BRDF models at a desert site, which showed that the Staylor–Suttles BRDF model [19] had the best fitting

accuracy and the kernel model [20] was the second best. Therefore, a comparison between the Staylor–Suttles and the kernel BRDF models is carried out at four different AERONET sites (Fowlers_Gap, Mezaira, and Tamanrasset_INM, and Dalanzadgad) based on the method of Bhatt et al. [21]. In this comparison, the reflectance of long time series from different models is normalized. The normalized result is shown in Figure 2. The information of the four AERONET sites is listed in Table 2.

- (3). The TOA reflectance observed from MODIS in the blue band (459–479 nm) over the four different AERONET sites were normalized by the Staylor–Suttles and the kernel BRDF models in 2018 and the mean/standard deviation pairs (Staylor–Suttles, kernel) for the four sites are (1.0069/0.0852, 1.0072/0.0936), (1.0047/0.0613, 1.0025/0.1090), (1.0015/0.0430, 1.0014/0.0464), and (1.0163/0.0563, 1.0077/0.0580) respectively. The comparison between the Staylor–Suttles and the kernel BRDF models at the red band is also carried out at the four AERONET sites, and the mean/standard deviation pairs (Staylor–Suttles, kernel) for the four sites at the red band are (1.0009/0.0307, 1.0005/0.0247), (1.0004/0.0240, 1.0004/0.0135), (1.0005/0.0227, 1.0005/0.0313), and (1.0026/0.0505, 1.0116/0.0336), respectively. The fitting accuracy of the Staylor–Suttles model is much better than that of the kernel model at Fowlers_Gap (the first one) and the fitting accuracy is very similar at the other three sites. Thus, the Staylor–Suttles model is strongly recommended in this study and the kernel model is also recommended in most cases.



(a)



(b)

Figure 2. Cont.

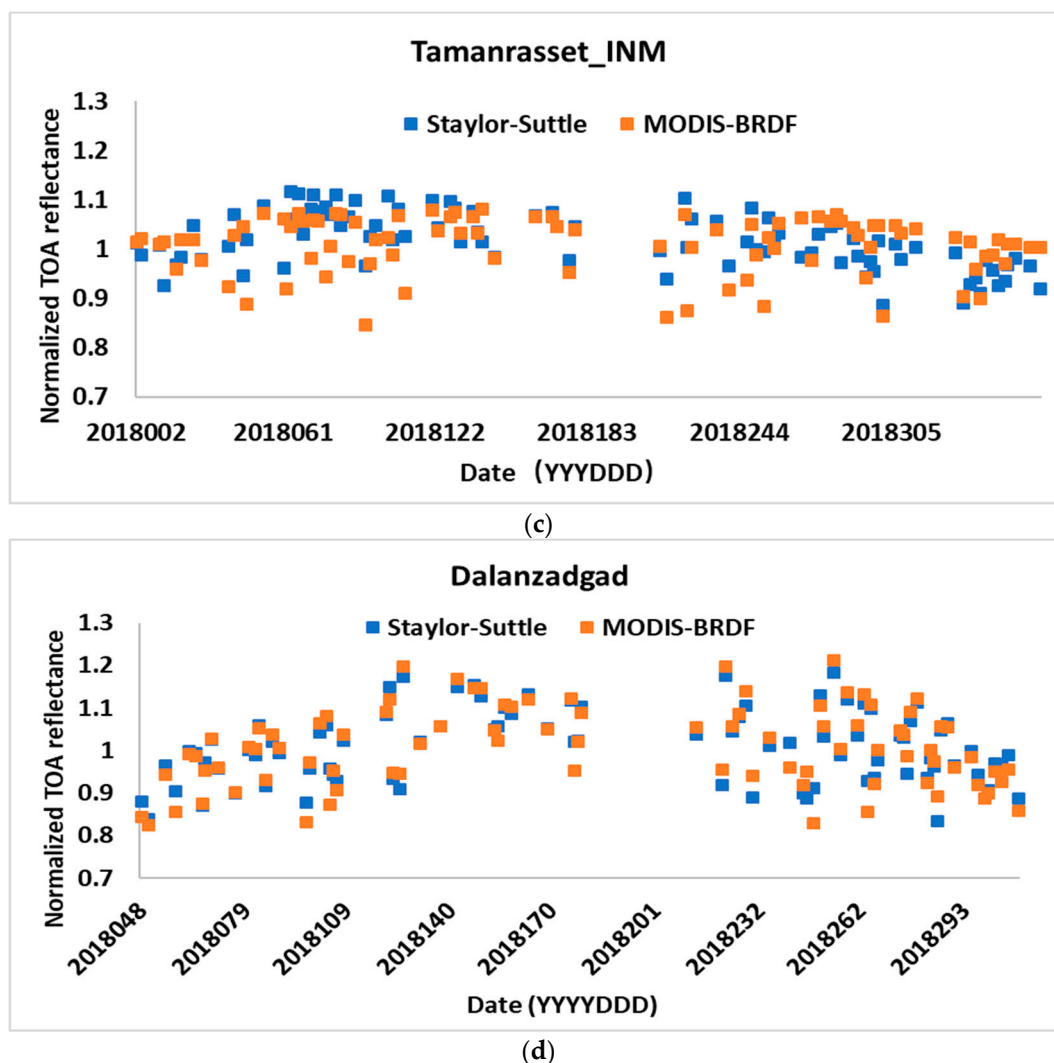


Figure 2. The bidirectional reflectance distribution factor (BRDF) fitting accuracy comparison between the Staylor–Suttler and the kernel BRDF models at four different AERONET sites around the world (a) Fowlers_Gap, (b) Mezaira, (c) Tamanrasset_INM, and (d) Dalanzadgad.

Table 2. The information of the four AERONET sites (Fowlers_Gap, Mezaira, and Tamanrasset_INM, and Dalanzadgad). (This information comes from <https://aeronet.gsfc.nasa.gov/>).

Site_Name	Longitude (°)	Latitude (°)	Elevation (m)	Average AOD Level 2.0 (AOD_500 nm) in 2018	Average Water Vapor in 2018 (g/cm ²)	Surrounding Surface Type
Fowlers_Gap	141.700820	−31.086300	181	0.0320	1.2355	Gobi
Mezaira	53.754660	23.104520	201	0.3078	1.3620	Gobi
Tamanrasset_INM	5.530000	22.790000	1377	0.1943	0.6060	Desert
Dalanzadgad	104.419167	43.577222	1470	0.0863	0.6667	Gobi-desert

2.2.2. Aerosol Optical Depth (AOD) Determination for ‘Clearest’ Days

The prerequisite for BRDF construction is to determine the AOD for the “clearest” days. Since over 10 years’ ground measurements of aerosol parameters including AOD have been recorded by AERONET, a worldwide aerosol observing network, the lowest AODs for different region can be retrieved through simple statistics from time series of AODs based on the ground measurements from the closest AERONET site or the site with similar geographic characteristics. The requirements for the

lowest AOD include: (1) the AOD needs to be as low as possible; (2) the number of measurements corresponding to the lowest AODs need to be enough for accurate BRDF construction. Figure 3 shows the AOD variations in multiple years based on the ground measurements from four different AERONET sites (Fowlers_Gap, Mezaira, Tamanrasset_INM, and Dalanzadgad from top to bottom) around the world. The determination of AOD for the clearest days is straightforward and they are 0.01, 0.05, 0.02, and 0.03, respectively, for the four sites.

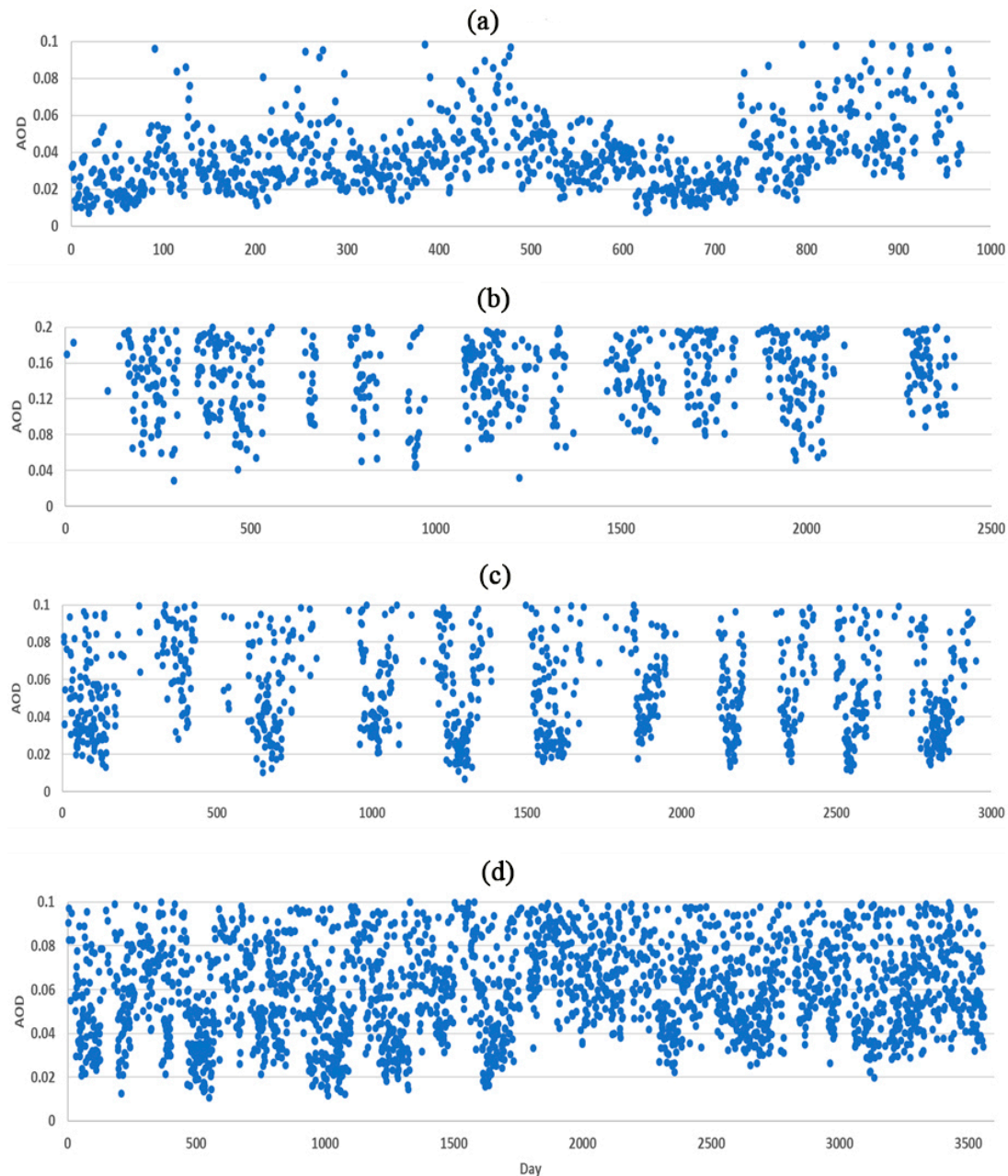


Figure 3. The AOD variations in multiple years based on the ground measurements from four different AERONET sites around the world (a) Fowlers_Gap, (b) Mezaira, (c) Tamanrasset_INM, and (d) Dalanzadgad.

2.2.3. Creation of the Look-Up Tables (LUTs)

Radiative transfer equation resolving is required for both the AOD retrieval and atmospheric correction; however, it is a very time-consuming procedure and it is impossible to do this on-line for

remote-sensing imagery. Therefore, the look-up table (LUT) method [22–24] which calculates different atmospheric quantities off-line by predefined parameters' settings is employed and each output from radiative transfer model, such as Second Simulation of a Satellite Signal in the Solar Spectrum (6S) [25], is listed regularly in a table. Subsequently, the output for each pixel of an imagery can be retrieved by searching the table using the parameters' information from the imagery. The 6S is used in this study for building up the LUT. The settings of the 6S's parameters are listed in Table 3.

Table 3. The settings of 6S's parameters to create look-up tables (LUTs) for AOD retrieval and atmospheric correction.

Parameter	Setting	Format	Source
View zenith angle	0–30°:5°	Range: interval	Metadata of MHSR imagery
Solar zenith angle	0–50°:5°	Range: interval	Metadata of MHSR imagery
Relative azimuth angle	0–180°:10°	Range: interval	Metadata of MHSR imagery
Atmospheric model	Mid-latitude summer, mid-latitude winter, tropical		Geographic latitude
Aerosol model	Desert and continental models		Land cover from FROM-GLC ¹
AOD	0.01, 0.05, 0.1, 0.2, 0.4, 0.8, 1.0, 1.5, and 2.0.		
Altitude	0, 100, 200, 500, 1000, 2000, 3000, 4000, and 5000 m		ASTER digital elevation model (http://asterweb.jpl.nasa.gov/gdem.asp)
Water vapor	0.1–5.1: 1 g/cm ² Blue: 0–0.2:0.02	Range: interval	MODIS product
Surface reflectance	Green: 0–0.4:0.04 Red: 0–0.4:0.04 NIR: 0–0.5:0.05	Range: interval	
Sensor	All the sensors listed in Table 1		Metadata of MHSR imagery

¹ Land cover from FROM-GLC is cited from [1]. Abbreviations: FROM-GLC, Finer resolution observation and monitoring of global land cover product.

3. Results and Validation

3.1. Atmospheric Correction Results

A large number of MHSR data have been used for testing the proposed method to demonstrate its effectiveness. Among these data, two datasets are selected as two examples for demonstrating the spatial and temporal consistency and the capability of different satellite data. Firstly, Figure 4 gives an example of the atmospheric-corrected images for different MHSR images with varied aerosol loadings. The different MHSR images include GF-1/WFV3, GF-1/WFV4, Landsat8/OLI, and Sentinel2B/MSI from top to bottom, respectively. In addition, the highly varied aerosol loadings and unevenly distributed aerosols of images in Figure 4 are well corrected; therefore, the example in Figure 4 comprehensively shows the capability for different satellite data and the ability to keep spatial consistency under different atmospheric conditions and even with unevenly distribution of aerosols at arid areas. The parameters of these images are listed in Table 4. Secondly, Figure 5 shows an example of a multi-temporal atmospheric correction of Landsat8/OLI at Tamarrasset_INM site with highly different aerosol loadings. The dates of these images are 29 May 2015, 1 December 2016, 19 February 2017, 23 March 2017, and 11 June 2017 from top to bottom, respectively. The parameters of these images are listed in Table 5. The images after atmospheric correction (the right column) are consistent in space and time. The images at 29 May 2015, and 11 June 2017 looks different because the very bright clouds influences the visual details of the two images. However, the uneven distribution of the aerosol is corrected very well, which shows the applicability of the proposed method.

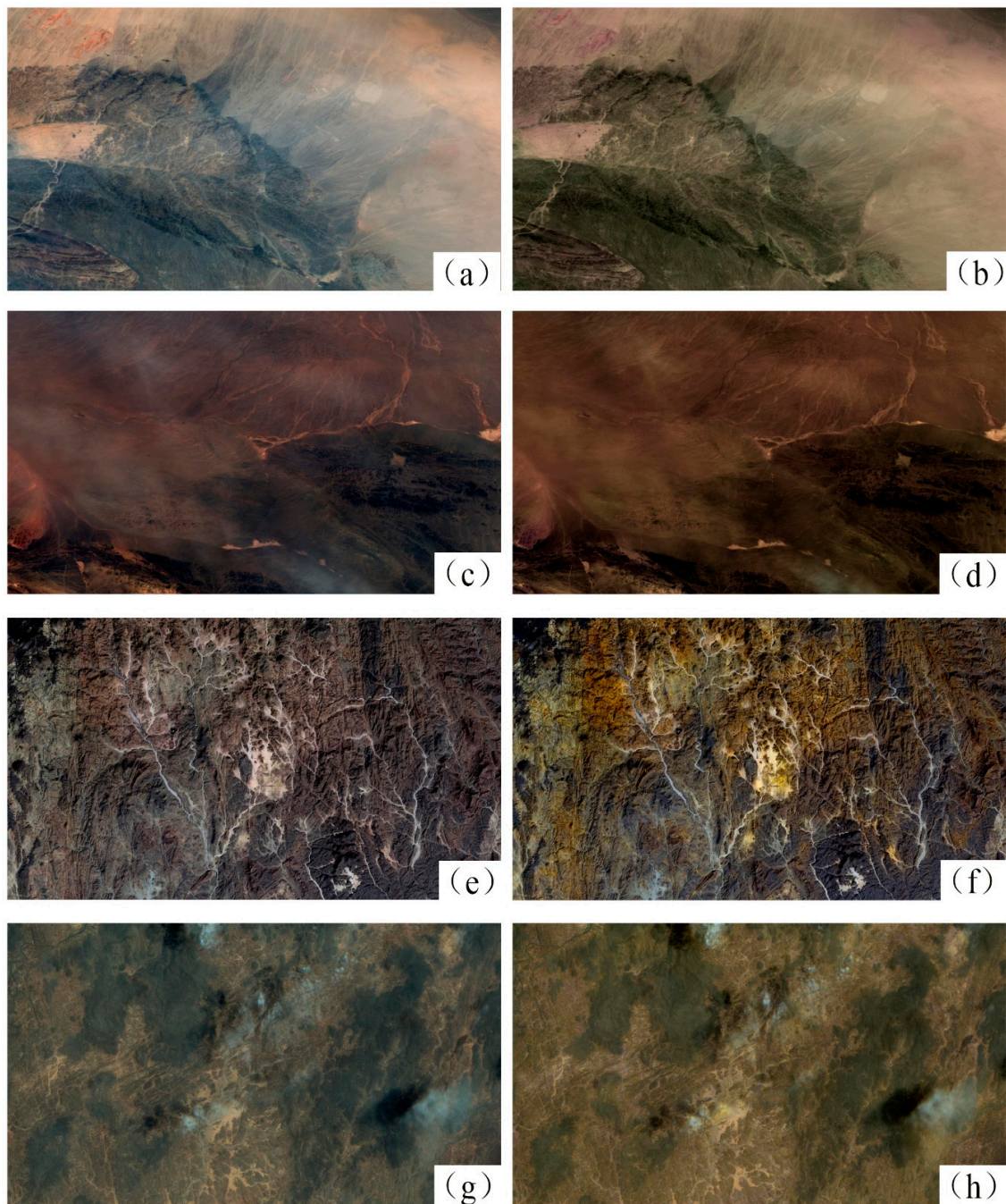


Figure 4. The atmospheric correction examples for the 4 different categories of MHSR imagery at 2 different AERONET sites. The four examples from top to bottom respectively are (a,b) GF-1/WFV3 at Dalanzadgad, (c,d) GF-1/WFV4 at Dalanzadgad, (e,f) Landsat8/OLI at Tamanrasset_INM, and (g,h) Sentinel2B/MSI at Tamanrasset_INM. Each of the 4 examples include two panels. The left column is the true color composite before atmospheric correction and the right column is the true color composite after the atmospheric correction.

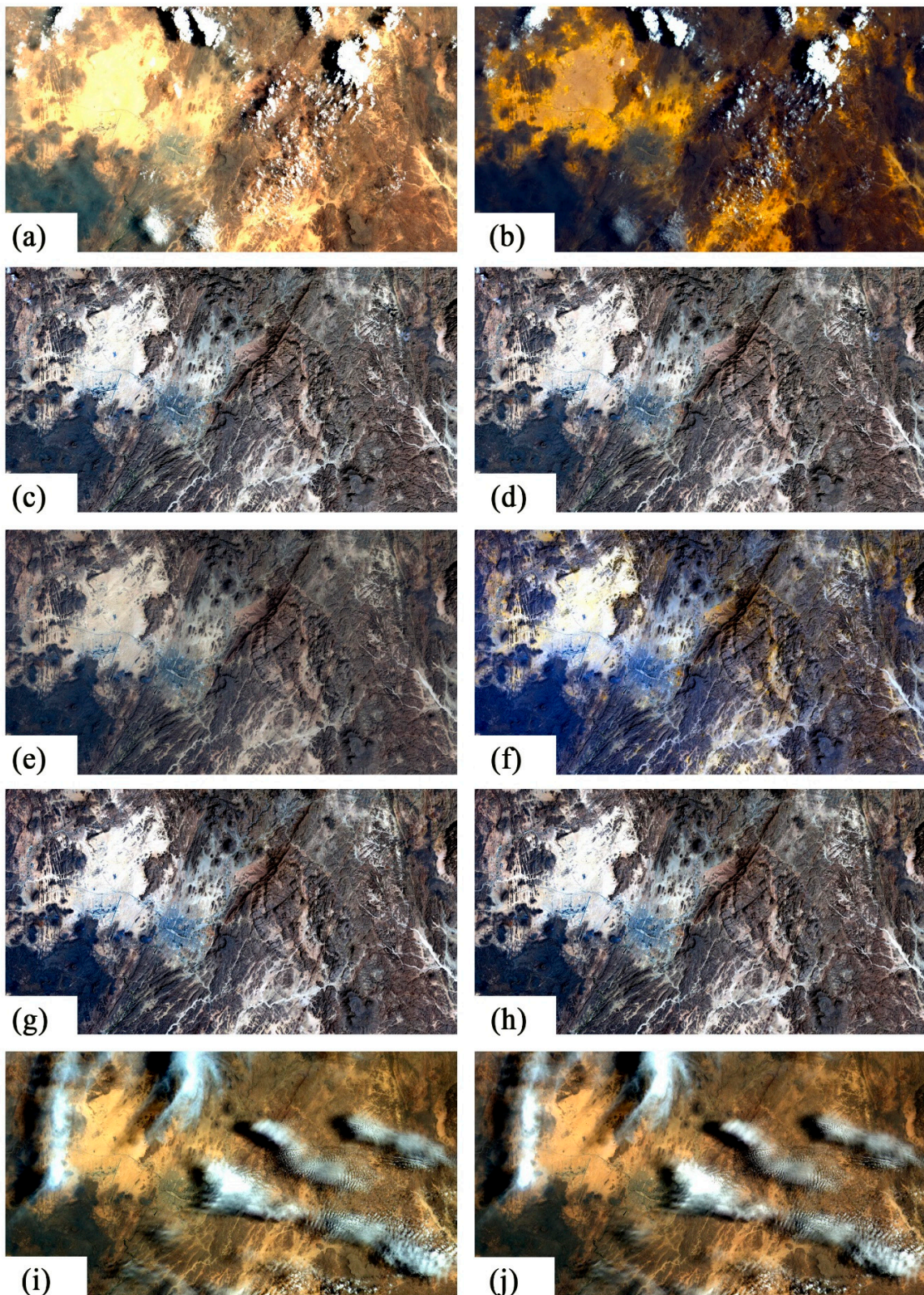


Figure 5. The atmospheric correction example for multi-temporal Landsat8/OLI imagery at Tamanrasset_INM site. The left column is the true color composite before atmospheric correction. The right column is the true color composite after atmospheric correction. The dates of these images from top to bottom respectively are (a,b) 29 May 2015, (c,d) 1 December 2016, (e,f) 19 February 2017, (g,h) 23 March 2017, and (i,j) 11 June 2017.

Table 4. The parameters of images in Figure 4.

Parameter	(a) and (b)	(c) and (d)	(e) and (f)	(g) and (h)
Image date	31 May 2018	31 May 2018	19 February 2017	24 May 2018
View zenith angle (°)	8.78	26.58	0	3.99
Solar zenith angle (°)	22.38	21.61	43.18	16.45
Relative azimuth angle ¹ (°)	116.15	112.75	139.62	157.16
Atmospheric model	Mid-latitude, summer	Mid-latitude, summer	Mid-latitude, winter	Mid-latitude, summer
Aerosol model	Continental	Continental	Continental	Continental
AOD	0.15	0.12	0.24	0.71
Altitude (m)	1569	1545	774	772
Surface reflectance	0.117	0.098	0.12	0.142
Sensor	GF-1/WFV3	GF-1/WFV4	Landsat8/OLI	Sentinel2B/MSI

¹ Relative azimuth angle = absolute (solar azimuth–sensor azimuth line-of-sight).

Table 5. The parameters of images in Figure 5.

Parameter	(a) and (b)	(c) and (d)	(e) and (f)	(g) and (h)	(i) and (j)
Image date	29 May 2015	1 December 2016	19 February 2017	23 March 2017	11 June 2017
View zenith angle (°)	0	0	0	0	0
Solar zenith angle (°)	21.34	49.28	43.18	32.79	21.49
Relative azimuth angle ¹ (°)	89.47	154.47	139.62	128.42	85.37
Atmospheric model	Mid-latitude, summer	Mid-latitude, winter	Mid-latitude, winter	Mid-latitude, winter	Mid-latitude, summer
Aerosol model	Continental	Continental	Continental	Continental	Continental
AOD	1.16	0.25	0.24	0.15	1.2
Surface reflectance	0.132	0.15	0.12	0.14	0.13

¹ Relative azimuth angle = absolute (solar azimuth–sensor azimuth line-of-sight).

Based on the above two examples and manual checking of more than 1000 atmospheric-corrected MHSR images, it can be concluded that the proposed method is capable of atmospherically correcting most of the MHSR imagery in arid areas with bright and stable surfaces with large varied aerosol loadings and with unevenly aerosol distribution (see line (a, b), (c, d) and (g, h) in Figure 4) and the spatial and temporal consistency after atmospheric correction is excellent.

3.2. Validation

Landsat8/OLI, Sentinel2/MSI and GF1/WFV from the US, ESA, and China, respectively, are selected for validation, since they have observations long enough and better radiometric capability. AOD values derived from Landsat8/OLI, Sentinel2/MSI and GF1/WFV images at four AERONET sites with bright and stable surface are compared with ground-measured AOD from the corresponding AERONET sites and the four sites are Dalanzadgad, Fowlers_Gap, Mezaira, and Tamanrasset_INM (Table 2). In order to better validate the algorithm, all images from the three sensors since launched have been collected. The total number of collected images is 1531.

For Landsat/OLI imagery, 723 images from 2013 to 2019 are retrieved for the four validation sites and only 136 corresponding measurements of AOD from AERONET are collected. The comparison between the retrieved AOD and the observed AOD is shown in the top left plot of Figure 6 and the statistics including the R^2 value, the mean of retrieved AOD, and the RMSE are 0.8929, 0.1138, and 0.0613, respectively, which shows that the retrieved AOD agrees very well with AERONET measurements. In addition, 87.5% of the discrepancy between the derived AOD and the measured AOD is less than 0.1, which is very low.

For Sentinel2/MSI imagery, 733 images from 2015 to 2019 were retrieved for the four validation sites and only 276 corresponding measurements of AOD from AERONET were collected. The comparison between the retrieved AOD and the observed AOD is shown in the top right plot of Figure 6 and the statistics including the R^2 value, the mean of retrieved AOD, and the RMSE are 0.7372, 0.2313,

and 0.1073, respectively, which shows that the retrieved AOD agrees also very well with AERONET measurements; 70.0% of the discrepancy between the derived AOD and the measured AOD is less than 0.1.

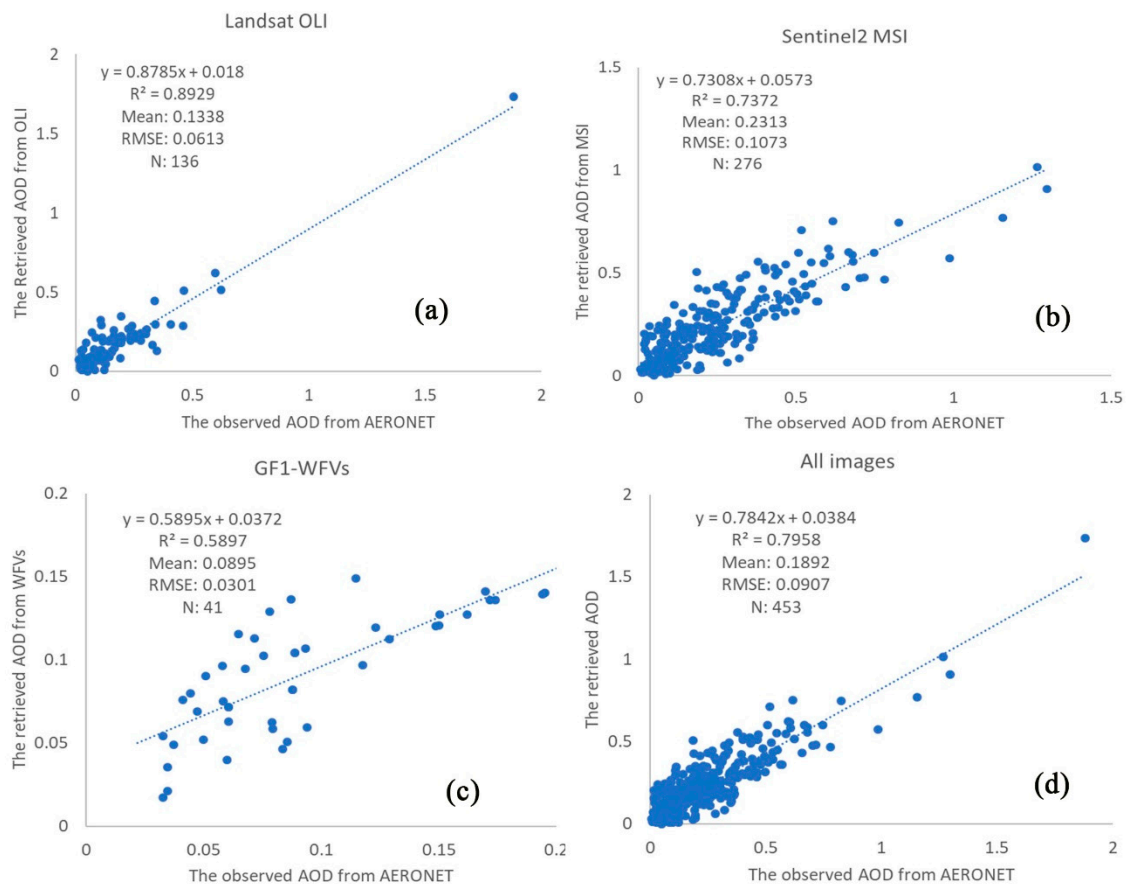


Figure 6. The validation of the retrieved AOD using 4 AERONET sites' measurements around the world. The plots from the top left to the bottom right are the validation for (a) Landsat/OLI, (b) Sentinel2/MSI, (c) GF-1/WFV, and (d) all images from all the three sensors, respectively.

Because they lack overseas satellite data-receiving stations, the Chinese satellites can only cover China and its surrounding areas; subsequently, for GF1/WFV imagery, only 81 images from 2018 to 2019 are retrieved at Dalanzadgad site alone and only 41 corresponding AOD measurements from Dalanzadgad AERONET site are collected. The comparison between the retrieved AOD and the observed AOD is shown in the bottom left plot of Figure 6. However, the R^2 value is only 0.5897, the AOD discrepancy is lower than 0.05, which is very small. The mean of retrieved AOD and the RMSE are 0.0895 and 0.0301 respectively. Because Dalanzadgad is far away from cities, the aerosol loading is very small and very small errors will bring very high uncertainty, which will degrade the correlation; subsequently, the RMSE is a better indicator for retrieving accuracy evaluation at this site instead of R^2 value.

All the data from all the three sensors and all the four sites are plotted in the bottom right plot in Figure 6 and it shows a very good agreement between the observed and the retrieved AOD. The R^2 value is very close to 0.8 and the RMSE is 0.0907.

The validation shows that AOD derived from the proposed method and the ground measurements from AERONET sites agree very well. The results from Landsat/OLI are the best among the three sensors and the reason is that Landsat/OLI is very close to nadir viewing. In addition, the data lacking at the other three sites of GF1 WFV degrades its validation and further investigation will be carried out in near future.

In order to better evaluate the performance of the proposed method, the validation for the AOD from the MODIS algorithm using ground-measured AOD from the above 4 AERONET sites has been done. For MODIS aerosol products over land, there are two algorithms: The dark target (DT) [8] and the deep blue (DB) [10] algorithms. The DT method assumes that there is a dark target area on the remote-sensing image to be corrected, the surface of this dark area has Lambert reflection characteristics, and the atmospheric condition of this dark area is uniform. On the premise of neglecting the multiple scattering of the atmosphere and the diffuse reflection of neighboring pixels, the reflectance of the dark target increases due to the influence of atmosphere, which is considered to be the effect of atmospheric range radiation. The DT method depends on the surface that is covered by dark targets, such as dense vegetation, water body, etc., which make the method doesn't suitable for other surfaces. The DB method uses the characteristics of strong atmospheric reflection and weak surface reflection in the blue band. The aerosol can be retrieved by substituting the surface reflectance of a clean day into the radiative transfer model. The DB method can be applied to most of the Earth's surface, such as vegetation, bare soil, water and even desert. For bright surfaces, the DT method usually fails and the DB method succeeds in retrieving aerosol information. In addition, the DT and DB have been combined (DB+DT) to refine the retrieved AOD and the AOD from the DB+DT method is more stable and accurate than that from the DB method only; subsequently, the retrieved AOD from the DB+DT method is used to undertake the validation. The left plot in Figure 7 shows the validation using all the retrieved AOD from both Aqua and Terra and all the validated AERONET sites, and the major indicators are the R² value (0.7643) and the RMSE (0.1181), which shows that the proposed method with higher R² value (0.7958) and lower RMSE (0.0907) is slightly better than the MODIS DB+DT method. Furthermore, most of the MHSR remote sensors are not equipped with the deep blue band and the DB method cannot be applied to these data; therefore, the proposed method is definitely more applicable. The retrieved AOD using the DB+DT method from both Aqua and Terra at Dalanzadgad site only is validated alone and it is presented in the right plot of Figure 7. It shows that the R² value is quite small and the RMSE is a better indicator for evaluating the performance of the AOD-retrieving algorithms at sites with very low aerosol loading. This is a similar phenomenon to the validation of GF1/WFV. The RMSE from GF1/WFV's retrieval (0.0301) is much smaller than that from MODIS's retrieval (0.0762).

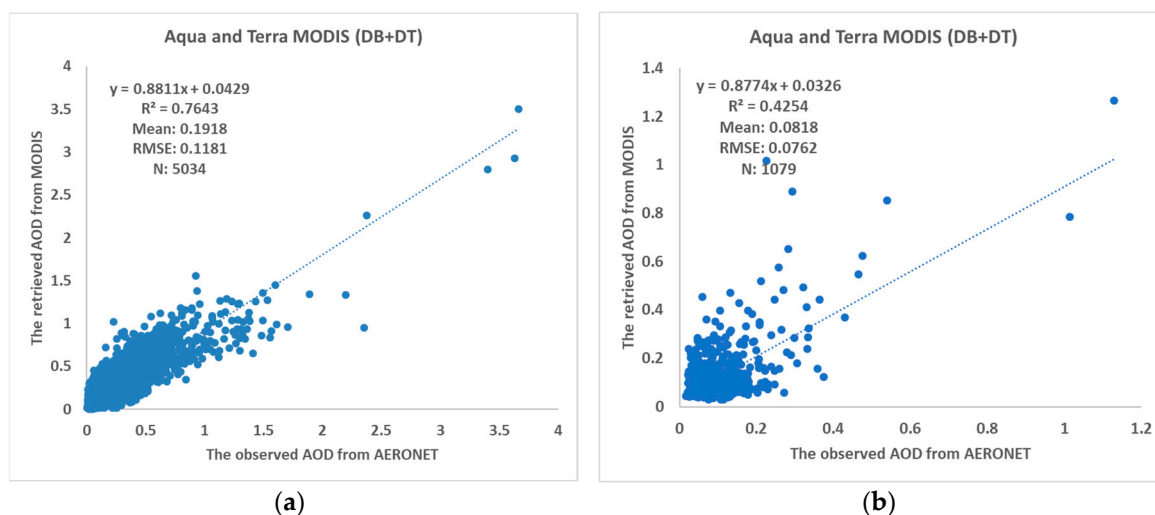


Figure 7. (a) The validation of the MODIS deep blue + dark target (DB+DT) algorithm using ground measured AOD from 4 AERONET sites around the world and (b) the validation for the MODIS DB+DT algorithm at Dalanzadgad site only (right). Note MODIS has observations twice daily, therefore it has a large number of data samples (~5000 in total). On the other hand, the revisiting period of Sentinel-2/MSI is 10-day before July 2017 and 5-day after July 2017, respectively. The ratios of the numbers of observations between MSI and MODIS are 1/20 and 1/10, respectively.

4. Discussion

The proposed method is specifically designed for bright and stable land surface, such as desert and the Gobi. In addition, the introduction of MODIS imagery greatly lowers the spatial resolution of the retrieved AOD and the applicability of the new method is subsequently restricted to those regions with relatively stable atmospheres; consequently, it cannot be applied to areas with highly varied atmospheres, such as urban areas and their surroundings.

The BRDF characterization fitting is the key step of the proposed method and the fitting accuracy of the Staylor–Suttles model is strongly recommended based on the four testing sites; however, the double verification of BRDF models is strongly suggested for better accuracy while applying the new method at other sites.

In the near future, the method will be applied to MODIS data at global scale and the retrieved AOD will be compared with that from the deep blue method.

5. Conclusions

In this study, a new atmospheric-correcting approach over bright and stable land surface, such as desert and the Gobi, for most of the MHSR imagery is developed. The major contributions of the new method include five aspects: (i) it takes consideration of the BRDF effect, so it can be applied to various MHSR remotely sensed imageries, especially for the Chinese MHSR imageries with very wide swath; (ii) it is specifically developed for bright and stable land surfaces; (iii) it is completely automatic; (iv) the deep blue band is not required, which is more applicable for most of the MHSR data; and (v) due to the relatively even distribution of the aerosol in the arid areas, the reduced spatial resolution of the retrieved AOD is accurate enough to capture the actual AOD distribution and greatly increases the efficiency. For the spatial expansion method [15], the initial AOD retrieved from the images in arid areas is rarely successful, so the spatial expansion procedure may fail or needs to be done iteratively, which is very time consuming; thus, the proposed algorithm will be an effective complement for the spatial expansion method in this situation. The derived AOD at four different locations around the world is validated with AERONET measurements at four sites (Fowlers_Gap, Mezaira, Tamanrasset_INM, and Dalanzadgad), which indicates that AOD estimated using the proposed method agrees very well with the AOD from the AERONET ground measurements. The AOD retrieved from Landsat8/OLI is the best among the three different sensors validated, which probably benefits from its nadir viewing design.

Author Contributions: B.Z. developed the algorithm and wrote the paper. S.W. wrote the program and produced the AOD from imagery. K.A. collected and processed the remote-sensing data. A.Y. compared the BRDF models. J.W. made the thematic maps of atmospheric correction. J.W. validated the results. X.G. and H.W. provided the Chinese Satellite data and did some preprocessing. Q.L. reviewed the manuscript and provided valuable suggestions. All authors have read and agreed to the published version of the manuscript.

Funding: This work was supported in part by the GF6 Project under Grant 30-Y20A02-9003-17/18 and the National Key R&D Program of China under Grant under Grant 2018YFA0605500 and 2017YFA0603000.

Acknowledgments: The GF1/WFV imagery used in this research is supported by the China Centre for Resources Satellite Data and Application (<http://www.cresda.com>). The Landsat8 OLI data were downloaded from the USGS website (<http://landsat.usgs.gov>). The Sentinel2 MSI data were downloaded from the ESA website (<https://earth.esa.int>). The AERONET data were downloaded from GSFC/NASA. The authors sincerely thank the reviewers who provided helpful comments to the manuscript.

Conflicts of Interest: The authors declare no conflict of interest.

References

1. Gong, P.; Wang, J.; Yu, L.; Zhao, Y.; Zhao, Y.; Liang, L.; Niu, Z.; Huang, X.; Fu, H.; Liu, S.; et al. Finer resolution observation and monitoring of global land cover: First mapping results with Landsat TM and ETM+ data. *Int. J. Remote Sens.* **2013**, *34*, 2607–2654. [[CrossRef](#)]

2. Hansen, M.C.; Potapov, P.V.; Moore, R.; Hancher, M.; Turubanova, S.A.; Tyukavina, A.; Tyukavina, D.; Thau, S.V.; Stehman, S.J.; Goetz, T.R.; et al. High-Resolution Global Maps of 21st-Century Forest Cover Change. *Science* **2013**, *342*, 850–853. [[CrossRef](#)]
3. Liang, S.; Fang, H.; Chen, M. Atmospheric correction of Landsat ETM+ land surface imagery. I. Methods. *IEEE Trans. Geosci. Remote Sens.* **2001**, *39*, 2490–2498. [[CrossRef](#)]
4. Ouaidrari, H.; Vermote, E.F. Operational atmospheric correction of Landsat TM data. *Remote Sens. Environ.* **1999**, *70*, 4–15. [[CrossRef](#)]
5. Masek, J.G.; Vermote, E.F.; Saleous, N.E.; Wolfe, R.; Hall, F.G.; Huemmrich, K.F.; Gao, F.; Kutler, J.; Lim, T.-K.A. Landsat surface reflectance dataset for North America, 1990–2000. *IEEE Trans. Geosci. Remote Sens. Lett.* **2006**, *3*, 68–72. [[CrossRef](#)]
6. Ju, J.; Roy, D.P.; Vermote, E.; Masek, J.; Kovalsky, V. Continental-scale validation of MODIS-based and LEDAPS Landsat ETM+ atmospheric correction methods. *Remote Sens. Environ.* **2012**, *122*, 175–184. [[CrossRef](#)]
7. Sun, L.; Sun, C.K.; Liu, Q.H.; Zhong, B. Aerosol optical depth retrieval by HJ-1/CCD supported by MODIS surface reflectance data. *Sci. China Earth Sci.* **2010**, *53*, 74–80. [[CrossRef](#)]
8. Remer, L.A.; Kaufman, Y.J.; Tanre, D.; Mattoo, S.; Chu, D.A.; Martins, J.V.; Li, R.R.; Ichoku, C.; Levy, R.C.; Kleidman, R.G.; et al. The MODIS aerosol algorithm, products, and validation. *J. Atmos. Sci.* **2005**, *62*, 947–973. [[CrossRef](#)]
9. Kaufman, Y.J.; Tanre, D.; Remer, L.A.; Vermote, E.F.; Chu, A.; Holben, B.N. Operational remote sensing of tropospheric aerosol over land EOS moderate resolution imaging spectroradiometer. *J. Geophys. Res.* **1997**, *102*, 17051–17067. [[CrossRef](#)]
10. Hsu, N.C.; Tsay, S.C.; King, M.D.; Herman, J.R. Aerosol properties over bright-reflecting source regions. *IEEE Trans. Geosci. Remote Sens.* **2004**, *42*, 557–569. [[CrossRef](#)]
11. Kaufman, Y.J.; Karnieli, A.; Tanre, D. Detection of dust over deserts using satellite data in the solar wavelengths. *IEEE Trans. Geosci. Remote Sens.* **2000**, *38*, 525–531. [[CrossRef](#)]
12. Tanre, D.; Legrand, M. On the satellite retrieval of Saharan dust optical thickness over land: Two different approaches. *J. Geophys. Res.* **1991**, *96*, 5221–5227. [[CrossRef](#)]
13. Luo, N.; Wong, M.S.; Zhao, W.; Yan, X.; Xiao, F. Improved aerosol retrieval algorithm using Landsat images and its application for PM10 monitoring over urban areas. *Atmos. Res.* **2015**, *153*, 264–275. [[CrossRef](#)]
14. Richter, R. A spatially adaptive fast atmospheric correction algorithm. *Int. J. Remote Sens.* **1996**, *17*, 1201–1214. [[CrossRef](#)]
15. Zhong, B.; Wu, S.; Yang, A.; Liu, Q. An improved aerosol optical depth retrieval algorithm for moderate to high spatial resolution optical remotely sensed imagery. *Remote Sens.* **2017**, *9*, 555. [[CrossRef](#)]
16. Liang, S.; Zhong, B.; Fang, H. Improved estimation of aerosol optical depth from MODIS imagery over land surfaces. *Remote Sens. Environ.* **2006**, *104*, 416–425. [[CrossRef](#)]
17. Zhong, B.; Yang, A.; Wu, S.; Li, J.; Liu, S.; Liu, Q. Cross-calibration of reflective bands of major moderate resolution remotely sensed data. *Remote Sens. Environ.* **2018**, *204*, 412–423. [[CrossRef](#)]
18. Zhong, B.; Liang, S.; Holben, B. Validating a new algorithm for estimating aerosol optical depths over land from MODIS imagery. *Int. J. Remote Sens.* **2007**, *28*, 4207–4214. [[CrossRef](#)]
19. Staylor, W.F.; Suttles, J.T. Reflection and emission models for deserts derived from nimbus-7 ERB scanner measurements. *J. Clim. Appl. Meteor.* **1986**, *25*, 196–202. [[CrossRef](#)]
20. Schaaf, C.B.; Gao, F.; Strahler, A.H.; Lucht, W.; Li, X.; Tsang, T.; Strugnell, N.C.; Zhang, X.; Jin, Y.; Muller, J.-P.; et al. First operational BRDF, albedo nadir reflectance products from MODIS. *Remote Sens. Environ.* **2002**, *83*, 135–148. [[CrossRef](#)]
21. Bhatt, R.; Doelling, D.R.; Morstad, D.; Scarino, B.R.; Gopalan, A. Desert-based absolute calibration of successive geostationary visible sensors using a daily exoatmospheric radiance model. *IEEE Trans. Geosci. Remote Sens.* **2013**, *52*, 3670–3682. [[CrossRef](#)]
22. Xu, Y.; Zhao, Q.; Chen, A. Lookup Table based Pixel-by-Pixel Atmospheric Correction Method of Remote Sensing Images. U.S. Patent CN101915914B, 24 October 2012.
23. Xu, Y.; Qin, Z.; Chen, A. A pixel-by-pixel atmospheric correction algorithm for MODIS data based on look-up table. *Geomat. Inf. Sci. Wuhan Univ.* **2010**, *35*, 959–962.

24. Hu, S.; She, X.; Tong, Q. Design and interpolation of a general look-up table for remote sensing image atmospheric correction. *J. Remote Sens.* **2014**, *18*, 45–60.
25. Kotchenova, S.; Vermote, E.R.; Matarrese, R.; Klemm, F., Jr. Validation of a vector version of the 6S radiative transfer code for atmospheric correction of satellite data. Part I: Path radiance. *Appl. Opt.* **2006**, *45*, 6762–6774. [[CrossRef](#)]



© 2020 by the authors. Licensee MDPI, Basel, Switzerland. This article is an open access article distributed under the terms and conditions of the Creative Commons Attribution (CC BY) license (<http://creativecommons.org/licenses/by/4.0/>).